J Mater Sci (2021) 56:12643–12659

Composites & nanocomposites

Mechanical, dynamic mechanical and thermal properties of TiO_2 nanoparticles treatment bamboo fiber-reinforced polypropylene composites

Juan Guo[2,3], Mengdan Cao[2], Wenting Ren[2], Hankun Wang[2], and Yan Yu[1,*]

[1] College of Material Engineering, Fujian Agriculture and Forestry University, Qishan Campus, Fuzhou City, Fujian 350108, People's Republic of China
[2] Institute of New Bamboo and Rattan Based Biomaterials, International Center for Bamboo and Rattan, Beijing 100102, People's Republic of China
[3] College of Mechanical Engineering, North China University of Science and Technology, Tangshan 063210, People's Republic of China

Received: 21 December 2020
Accepted: 10 April 2021
Published online: 3 May 2021

ABSTRACT

To obtain better interfacial bonding between bamboo fibers (BFs) and matrix polypropylene (PP), PP/BFs composites were prepared by means of modifying BFs with TiO_2 nanoparticles. The static mechanical and dynamic mechanical properties, thermal properties, morphology and water resistance of the fabricated composites were characterized. The results showed the static and dynamic mechanical properties, thermal stability and water resistance of the composite were all improved at different extents by the introduction of TiO_2 nanoparticles, especially with the addition of 0.4 wt% TiO_2 nanoparticles (PP/BF/T3). The performances enhancement of TiO_2 nanoparticles modified composites was mainly attributed to the interfacial bonding improvement, demonstrated by the Cole–Cole curves of dynamic mechanical analysis and the morphological analysis of fracture surface, as well as the increased crystallinity revealed with differential scanning calorimetry measurements.

Handling Editor: Chris Cornelius.

Address correspondence to E-mail: yuyan9812@outlook.com

https://doi.org/10.1007/s10853-021-06100-z

GRAPHICAL ABSTRACT

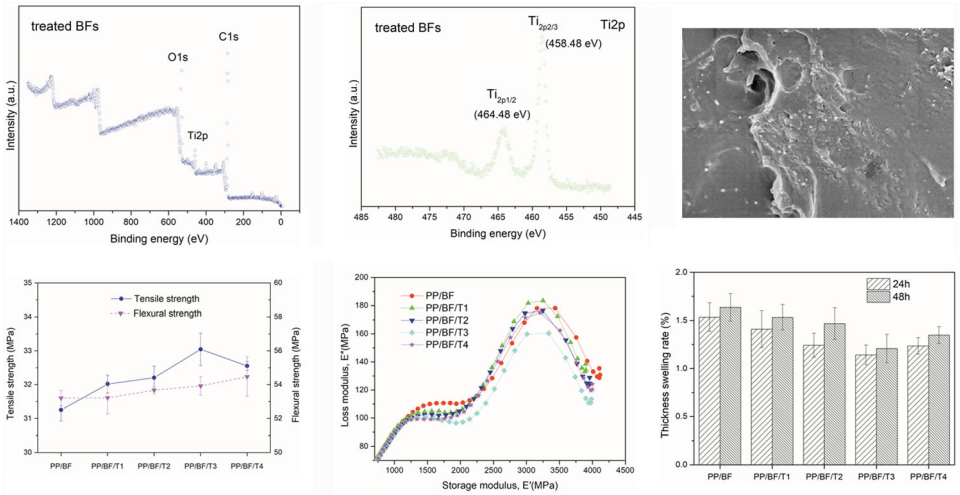

Introduction

Bamboo is a kind of renewable biomass raw material with abundant resources and great practical value. It has been widely used in construction and other fields due to its combined advantages of rapid growth rate, high strength and good toughness, etc. [1, 2]. Research and utilization of bamboo products have attracted a lot of attention in both academic and commercial circles in recent years [3–7]. However, with the vigorous development of bamboo processing industry, a large number of bamboo processing residues and wastes have been generated, which would result in serious environmental pollution and cost increase, if they were not rationally utilized. Therefore, it is vital to develop efficient approaches to make full use of these bamboo processing residues and wastes.

Bamboo-plastic composites (BPCs), which are manufactured by blending bamboo powders of different size with various polymer matrix along with applying appropriate processing technique (such as extrusion, injection molding and hot compressing), are considered to be one of the most effective approaches for bamboo processing residues and wastes [8–10]. Bamboo fibers (BFs) have been confirmed to be an excellent substitute for synthetic fiber (i.e., carbon fibers, glass fibers and organic fibers) in composite materials, due to their outstanding strength and stiffness, light weight, large aspect ratio, easy availability, natural biodegradability and environmental friendliness [11–14]. Therefore, a large number of BPCs have been extensively used in a variety of fields such as interior decoration, outdoor construction and automobile components, which improve the economic value of bamboo products as well as reduce the use of petroleum-based plastics [15–17].

Unfortunately, BFs contain a large number of highly hydrophilic hydroxyl groups, resulting in poor interface compatibility with nonpolar polymer matrix and poor dispersion uniformity in prepared BPCs. Many methods or processes have been proposed to improve the interfacial compatibility between BFs and polymer resin [18–21], typically by modification of BFs with chemical technologies such as alkalization [22, 23], coupling and grafting [24, 25], or physical ones such as hot water treatment [26], microwave irradiation [27], steam blasting and inorganic nanoparticle deposition [28, 29]. Among these methods, modification of BFs with inorganic nanoparticles suspension solution (such as calcium carbonate, silicon dioxide, talc) represents a very promising direction, owing to its surface effect, quantum scale effect, photocatalysis, mild treatment

conditions, and high feasibility, etc. [20, 30]. It has been reported that the PP/BFs composites with the application of various nanoparticles have the enhanced properties of thermal resistance [17], flame retardant [15], aging resistance and mould proof features [16] and so on. At the same time, the addition of nanoparticles into PP/BFs composites can improve the dispersion and uniformity of bamboo fibers in the matrix resin, resulting in enhanced excellent mechanical properties and dimensional stability. However, the properties of BPCs are largely dependent on the specific inorganic nanoparticle and application technique. Nano-TiO_2 represents one of the most commercially important inorganic nanoparticles but seldom applied to BPCs. Furthermore, although many research works have paid much attention on the characterization of surface performance of modified BFs based on their chemical composition, surface morphology and pull-out shear stress [31, 32], the quantitative characterization of the interface adhesion properties between BFs and polymer matrix in the BPCs has been to a large extent ignored.

In this paper, commercial nano-TiO_2 particles were dispersed by a self-made silane solution and applied to the surface of bamboo fibers by in situ solid phase grafting (by forming −O–H…bonds) through the so-called spraying technique. The modified bamboo fiber-reinforced polypropylene composites were then prepared with the injection molding process. The main objective of this paper was to study the interfacial compatibility between nano-TiO_2 modified bamboo fibers and polypropylene matrix. To address that, dynamic mechanical analysis (DMA) was carried out to quantitatively characterize the interface bonding between fibers and matrix in the BPCs. In addition, the fracture surface morphology, water absorption and thickness swelling of the samples were also explored as complementary evaluation of the effect of TiO_2 nanoparticles on the interface adhesion properties between BFs and matrix polymer.

Experimental section

Materials

The pure isotactic polypropylene pellets (T30S-iPP) with the density of 0.905 g/cm^3, a melt flow index of 3.5 g/(10 min), applied a matrix resin were purchased from Kunlun Petrochemical Co., Ltd. (Hohhot, China). They were dried in the oven at 80 °C for 4 h before use. Industrial bamboo fibers (BFs) [Phyllostachys edulis (Carr.) H. De Lehaie] (3–4 years old) with 100-mesh size were supplied by Sanmu Wood Technology (Hubei, China). BFs were washed with tap water to remove impurities and dried in an oven at 103 ± 2 °C until moisture content was less than 3 wt%. Rutile TiO_2 nanoparticles (40 nm in diameter) were purchased from Boyu Hi-tech New Materials Technology Co., Ltd. (Beijing, China) and were dried in vacuum at 103 ± 2 °C for 48 h before use. Ethyl alcohol (≥ 99.9%) and 3-methacryloxy propyltrimethoxysilane (KH-570) (≥ 98%) were purchased from Sinopharm Chemical Reagent Co., Ltd. (Beijing, China) and used as received.

Surface treatment of bamboo fibers

The surface of bamboo fibers was treated with nano-TiO_2 dispersion self-made in the laboratory. The process for the treatment of BFs was as follows: First, KH-570 reagent (2 g) was directly added into 100 mL ethanol solution, where the volume ratio of ethyl alcohol to purified water was 6:4. The mixed solution was then fully reacted with ultrasonic vibrations for 10 min to form a homogeneous silane solution. Second, the dried TiO_2 nanoparticles (0.1 g, 0.2 g, 0.4 g and 0.8 g) were dispersed in 50 mL ethyl alcohol through rapid agitation to make nano-TiO_2 suspension. Subsequently, the obtained suspension was added into the prefabricated silane solution drop by drop and stirred. The mixture was then completely dispersed by ultrasonic for 10 min to prepare nano-TiO_2 dispersion. In order to prevent the ultrasonic instrument (JY 99-II DN) from overheating, all experiments adopted the working mode of running for 3 s and stopping for 3 s with a power of 480 W. Finally, the nano-TiO_2 dispersion was evenly sprayed onto the surface of bamboo fibers with a watering can, which was then placed at room temperature for 7 days. After the ethanol solution was thoroughly evaporated, the treated BFs were dried in an oven at 103 ± 2 °C for 48 h and then stored in a zipper-sealed plastic bag for usage.

Preparation of the PP/BFs composites

The PP/BFs composites were fabricated via a process of melt-extruding and injection molding. Extrusion of the bamboo fiber and PP mixture was carried out using a co-rotating twin-screw extruder (HAAKE PolySoft Monitor, Made in Germany) with a constant screw rotation speed of 20 rpm. The barrel temperatures in three sections from hopper to die were 180, 185 and 175 °C, respectively. The extruded rods with a diameter of 3 mm were quenched in a water bath and then cut into pellets. The obtained pellets were dried in an oven at 80 °C for 12 h before injection molding. Mechanical testing samples based on ASTM Standard were prepared using injection molding (M1300D, Qi-en Science and Technology, Wuhan, China) at a temperature of 175 °C, an injection pressure of 6–7 MPa for 18 s and then cooled for 6 s. The formulations and codes of all samples are summarized in Table 1, and the schematic preparation of the nano-TiO_2 dispersion treatment BFs and the fabrication of PP/BFs composites are shown in Fig. 1.

Characterization of the bamboo fibers and PP/BFs composites

Element analysis of bamboo fibers

Element analysis on untreated and treated bamboo fibers was detected with X-ray photoelectron spectroscopy (XPS, ESCALAB 250Xi, Thermo Scientific) using monochromatized Al Ka X-ray source at a constant analyzer.

Physical and mechanical properties of the PP/BFs composites

The density of the PP/BFs composite boards was tested according to a Chinese national standard GB/T 17,657–2013[33] with three replications. Tensile strength, flexural strength and unnotched impact strength of the composites were measured according to ASTM D-638, ASTM D790 and ASTM D6110, respectively. Five different specimens were tested for every mechanical indicator at ambient conditions.

Table 1 The formulations of all premixed materials

Sample code	PP (wt%)	BFs (wt%)	Nano-TiO_2 (wt%)
PP/BF	65	35	0
PP/BF/T1	65	34.9	0.1
PP/BF/T2	65	34.8	0.2
PP/BF/T3	65	34.6	0.4
PP/BF/T4	65	34.2	0.8

Thermal properties of the PP/BFs composites

Differential scanning calorimetry (DSC) (Q100, TA Instruments, USA) was used to determine the thermal performances of the prepared composite samples in regard to crystallization and melting temperature. The specimens (5–8 mg) were encapsulated in hermetically sealed aluminum pans and heated from 30 °C to 200 °C (to remove any thermal history causing by extrusion and injection processing) and then kept isothermal for 5 min. Subsequently, they were cooled to 30 °C and then reheated to 200 °C. During these processes, the ramp rates for all of the cooling and heating cycles were 10 °C/min and the flowing of dry nitrogen gas was 50 mL/min [34].

Thermogravimetric analysis (TGA) (Q500, TA Instruments, USA) was applied to determine the thermal stability of samples. The specimens (5–8 mg) were placed in a platinum pan and heated from 30 °C to 700 °C at the ramp rate of 10 °C /min under dry nitrogen gas (flow rate 60 mL/min).

Dynamic mechanical analysis (DMA)

The dynamic mechanical behaviors of the samples were evaluated by means of dynamic mechanical analyzer (DMAQ800, TA Instruments, USA) under a double-cantilever bending mode according to ASTM D4065 standard. Storage modulus (E'), loss modulus (E'') and mechanical damping factor (tan δ) of the composite samples were described against temperatures.

Fracture surface morphology analysis

The fracture surface of the PP/BFs composites from the three-point bending tests was sputter-coated with gold under high vacuum (over 10^{-5} mbar) and then observed using a field emission scanning electron microscopy (FE-SEM, XL-30E, Philips B.V., Eindhoven, The Netherlands) operating at an accelerating voltage of 7 kV.

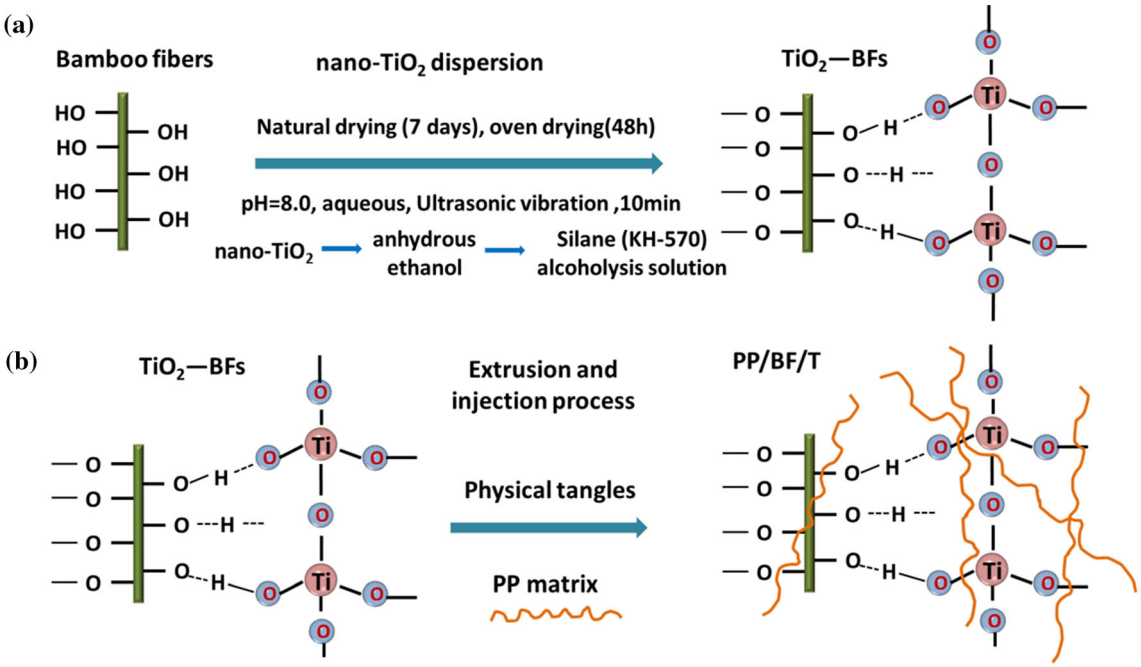

Figure 1 Schematic showing the preparation of **a** nano-TiO_2 dispersion treatment BFs, **b** PP/BFs composites.

Determination of water absorption and thickness swelling

Determination of water absorption (WA%) and thickness swelling (TS%) for PP/BFs composites was performed according to ASTM D570 [35].

Statistical analysis

The data for each mechanical property of the PP/BFs composites were statistically studied using the SPSS19.0 statistical. The one-way analysis of variance (ANOVA) was conducted to identify that there was a significant difference between the mean values according to least significant difference criteria with a 95% confidence level ($p < 0.05$).

Results and discussion

Evaluation on surface compositions of treated bamboo fibers

XPS spectrum was recorded to analyze the changes in chemical compositions on the BFs surface during modifications (Fig. 2). From the XPS spectra in Fig. 2a1, the surface elements of untreated BFs specimens mainly consist of carbon (C) and oxygen (O), whereas the surface of 0.4 wt% TiO_2 nanoparticles treated BFs mainly consist of carbon (C), oxygen (O) and titanium (Ti) (Fig. 2b1). In Fig. 2a1 and a2, untreated BFs displayed O1s signal at 532.78 eV and C1s signal at 286.13 eV, which were assigned to the C–O bonds and C–C bonds, respectively. After treated BFs with TiO_2 nanoparticles, in addition to the above two signals, an obvious Ti2p signal at 458.51 eV was observed in the treated BFs, which was clearly attributed to the titanium atoms in nanotitanium dioxide (Fig. 2b1). Deconvolution of the O1s peak in the XPS profile of treated BFs demonstrated two signals at 532.58 eV and 529.88 eV, corresponding to C–O bonds in cellulose and Ti–O structure in TiO_2 nanoparticles (Fig. 2b2). In Fig. 2b3, the Ti2p peaks of treated BFs located in 464.12 eV and 458.48 eV were originated from the Ti–O structure. Furthermore, the relative atomic content proportion of C/Ti/O changed from 67.38/0.32/32.3 to 61.78/2.18/36.03 after 0.4 wt% TiO_2 nanoparticle modification. The C/O atomic ratio was calculated to be 1.7 for treated BFs, which was lower than the value 2.1 for the untreated BFs. All the above results definitely confirmed the successful loading of TiO_2 nanoparticles onto the surface of BFs.

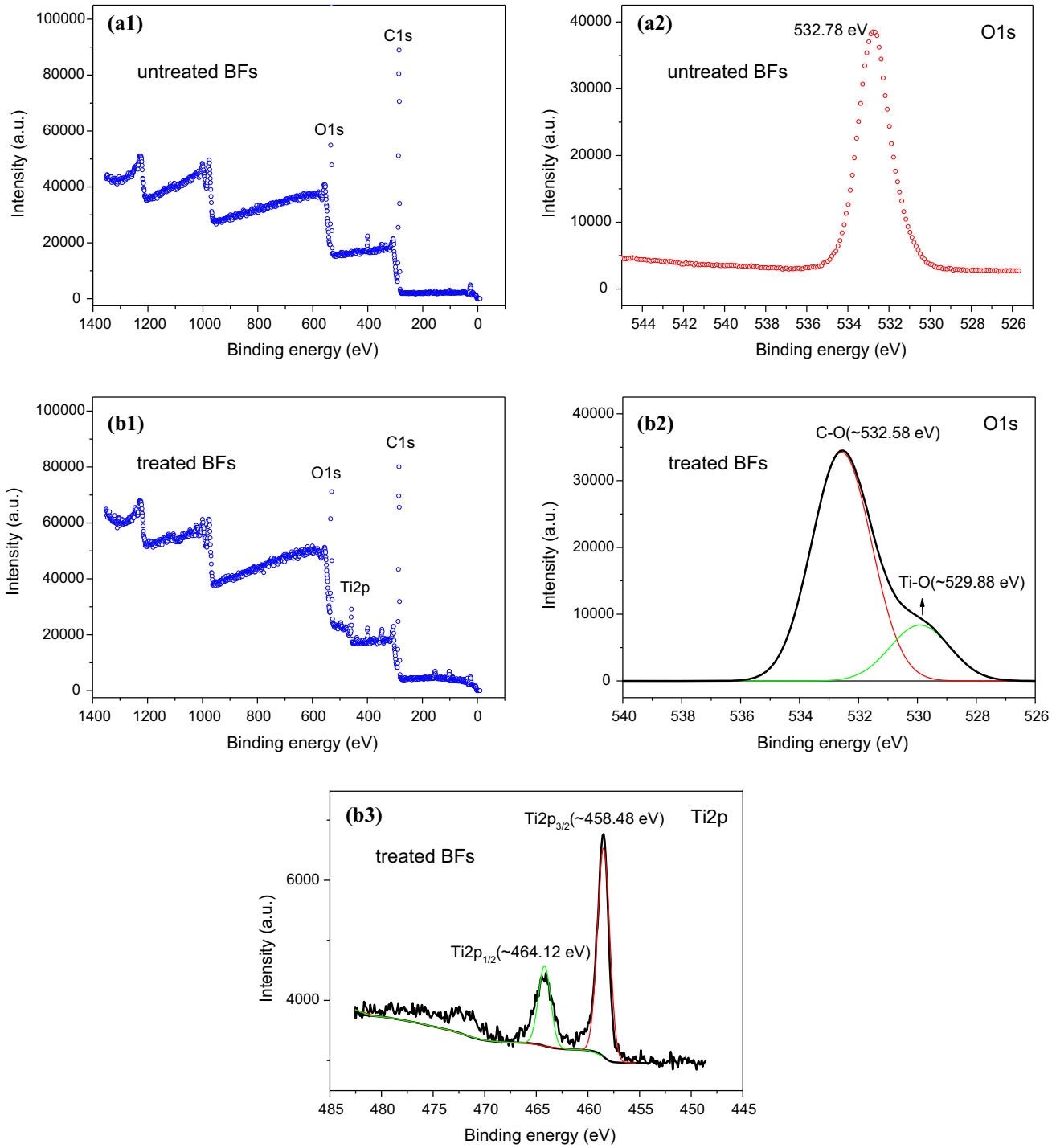

Figure 2 Survey XPS spectra of **a1** untreated BFs and **a2** O1s for untreated BFs, **b1** treated BFs, **b2** O1s for treated BFs and **b3** Ti2p for treated BFs.

Physical and mechanical properties of PP/BFs composites

The density values of PP/BFs composites at variable weight percentage of TiO_2 nanoparticles (0–0.8 wt%) are represented in Table 2 and Fig. 3. A slight but stable rising was observed in the values of density with increase in TiO_2 nanoparticles content from 0 to 0.8 wt%. This should be attributed to the addition of small amount (<1.0 wt%) of TiO_2 nanoparticles with

Table 2 Physical and mechanical properties of PP/BFs composites

Sample name	Density (g/cm^3)	Tensile strength (MPa)	Flexural strength (MPa)	Impact strength (KJ/m^2)
PP/BF	1.0125c (± 0.003)	31.252c (± 0.332)	53.209a (± 0.450)	7.667a (± 0.169)
PP/BF/T1	1.0145b (± 0.009)	32.016b (± 0.260)	53.222a (± 0.955)	8.532a (± 0.157)
PP/BF/T2	1.0154b (± 0.003)	32.207b (± 0.340)	53.670a (± 0.211)	8.105a (± 0.567)
PP/BF/T3	1.0180a (± 0.009)	33.045a (± 0.478)	53.923a (± 0.540)	8.010a (± 0.156)
PP/BF/T4	1.0196a (± 0.009)	32.555ab (± 0.129)	54.472a (± 1.168)	7.946a (± 0.740)

Note The numerical value in the parenthesis represents standard deviation. Different letters indicate significantly different groups ($p < 0.05$)

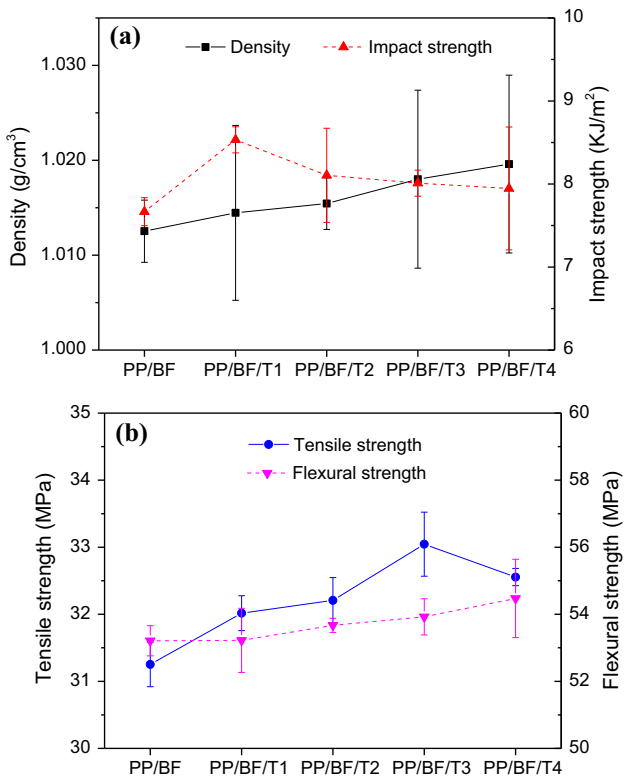

Figure 3 Physical and mechanical properties for PP/BFs composites with different contents of TiO_2 nanoparticles: **a** samples' density and impact strength, and **b** tensile strength and flexural strength.

higher density. The tensile properties of PP/BFs composites as a function of increasing TiO_2 nanoparticles loading are shown in Fig. 3b. There was some increase in the tensile strength of the PP/BFs composites with the incorporation of TiO_2 nanoparticles. The PP/BF/T3 composite performed the highest tensile strength of 33.045 MPa, increased by 5.74% compared to the PP/BF composite (Table 2). Furthermore, a slight increase in flexural strength was observed with the increase in TiO_2 nanoparticles (Fig. 3b). The flexural strength in case of PP/BF composite was 53.209 MPa, which increased to 54.472 MPa at 0.8 wt% TiO_2 nanoparticles content (Table 2). There were mainly two reasons for this phenomenon. On the one hand, the surface roughness of rigid BFs could be improved by the addition of TiO_2 nanoparticles, which is beneficial for increasing the contact area between the BFs and matrix resin. On the other hand, the TiO_2 nanoparticles played a positive role in improving matrix–fiber interaction, leading to form a strong mechanical interlocking and a reinforced polymer matrix, which was consistent with the results reported in the literature [35].

The unnotched impact strength values of PP/BFs composites with variation in TiO_2 nanoparticles loading from 0 to 0.8 wt% are listed in Table 2, and corresponding data are plotted in Fig. 3a. The impact strength of PP/BFs/T1 composites at 0.1 wt% TiO_2 nanoparticles loading achieved a peak value 8.532 kJ/m^2 (11.28% higher than that of PP/BF composite), but decreased with the further increase in the TiO_2 nanoparticles loading. The improvement of impact resistance of PP/BFs/T1 composites could be due to the enhancement of the interfacial adhesion between BFs and matrix resin, which was in accordance with the above result. However, excessive TiO_2 nanoparticles loading also implies higher probability of stress concentration in the composites, resulting in lower impact strength of the samples. Similar results were reported by the literature [36].

Thermal properties

Differential scanning calorimetry (DSC)

The DSC thermograms recorded during crystallization and melting of the PP/BFs composites are shown

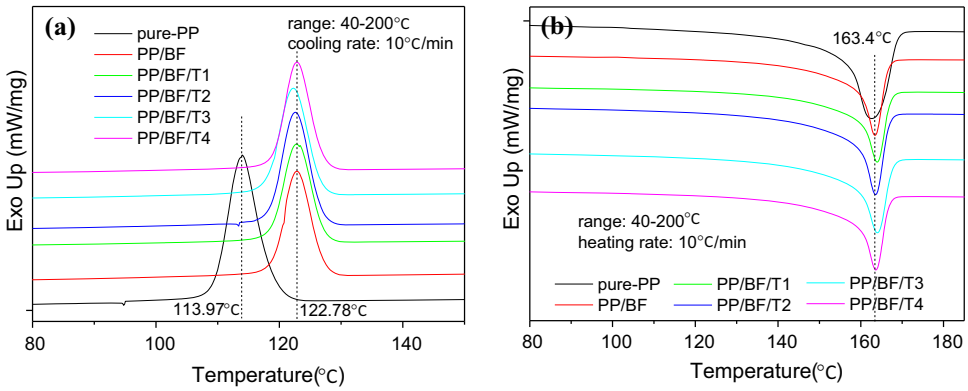

Figure 4 DSC curves of the PP/BFs composites: **a** cooling process, **b** the second heating process.

Table 3 Parameters of melting and crystallization properties for PP/BFs composites

Sample	T_c (°C)	T_m (°C)	ΔH_c (J/g)	ΔH_m (J/g)	X_c (%)
Pure-PP	113.97	162.67	86.53	54.89	40.40
PP/BF	122.78	163.40	53.45	31.29	23.03
PP/BF/T1	123.12	163.58	52.11	31.5	23.19
PP/BF/T2	122.94	163.45	59.94	33.71	24.81
PP/BF/T3	122.51	163.74	56.74	35.14	25.87
PP/BF/T4	122.53	163.35	54.31	31.67	23.31

in Fig. 4a, b, and the key parameters obtained from these DSC curves are summarized in Table 3. Parameters T_c and ΔH_c of the pure PP and PP/BFs composites were taken as the crystallization peak temperature and the corresponding crystallization exotherm from the cooling cycle (Fig. 4a), whereas T_m and ΔH_m were taken as the melting peak temperature and the melting endotherm from the second heating process (Fig. 4b), respectively. The relative of crystallinity was calculated using Eq. (1) in ESM. It was found that the addition of BFs and TiO_2 nanoparticles in PP matrix resulted in a significant increase in the T_c of PP matrix about 9 °C, and a slight increase in the T_m of PP matrix, which was possibly due to the heterogeneous nucleation effect of BFs, as well as the interface enhancement between the BFs and matrix with the incorporation of TiO_2 nanoparticles. However, the X_c values depicted in Table 3 revealed that the degree of crystallinity decreased significantly, such as the X_c value of pure PP was 40.40%, whereas it decreased to 23.03% for the PP/BF composite. This reduction was related to the transcrystalline region in which the lateral growth of spherulites was restricted in due to the presence of BFs. Nevertheless, in regard to different content of TiO_2 nanoparticles treated BFs, the X_c values of PP/BFs composites increased slightly to 25.87% for the PP/BF/T3 composite. This behavior might be due to the enhanced interfacial interaction between the BFs and PP matrix that promoted the crystallization phase of matrix polymer, which is similar to the results obtained by Satapathy et al. [35] in case of banana fiber/recycled high-density polyethylene biocomposites.

Thermogravimetric analysis (TGA)

The thermal stability of the PP/BFs composites in a nitrogen atmosphere was performed by TGA with the results shown in Fig. 5a, b, and the parameters obtained are listed in Table 4. The onset thermal decomposition temperature (T_{onset}) was taken as the temperature at 5% weight loss, and the maximum thermal decomposition rate temperature (T_{max}) corresponded to the peak temperature of DTG curves. We found from Fig. 5a, b and Table 4 that the T_{onset} of PP/BFs composites was reduced compared with that of pure PP matrix caused by the lower onset thermal decomposition temperature of hemicellulose in BFs. However, the final decomposition temperatures (T_f) of the PP/BFs composites increased by 11.4–17.6 °C, and the peak values of decomposition rate decreased significantly against pure PP, which confirmed that the thermal stability of PP/BFs composites was increased. In addition, Fig. 5b presents two thermal decomposition stages: one was the weight loss at about 355 °C corresponded to the degradation of BFs, whereas the second stage at about 450 °C indicates the degradation of PP matrix. However, the thermal decomposition temperature in both the stages for the PP/BFs composites was comparatively lower (about 6–8 °C) than that of the PP/BF composite. This

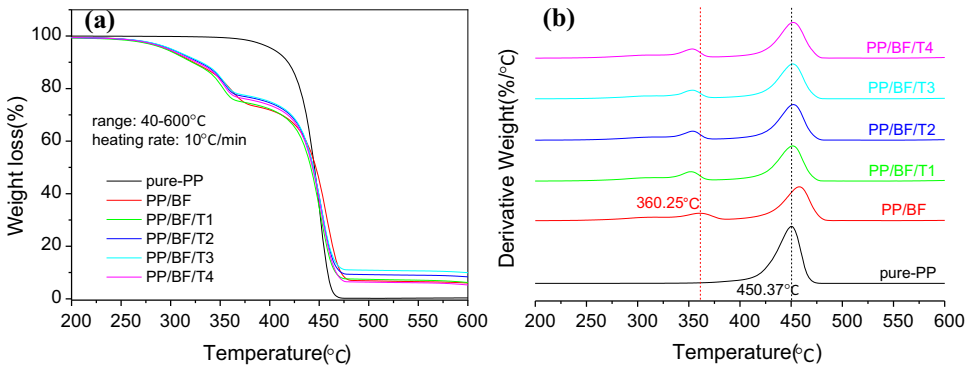

Figure 5 The thermal decomposition behaviors of the PP/BFs composites: **a** TG curves, **b** DTG curves.

Table 4 Parameters of the thermogravimetric analysis for PP/BFs composites

Sample	T_{onset} (°C)	$T_{50\%}$ (°C)	$T_{max\text{-}BF}$ (°C)	$T_{max\text{-}c}$ (°C)	T_f (°C)	W_r (%)
Pure-PP	403.15	445.20	–	450.37	463.12	0.35
PP/BF	296.77	446.59	360.25	457.78	480.79	6.01
PP/BF/T1	295.03	441.55	351.82	451.61	474.53	6.19
PP/BF/T2	300.40	443.95	353.64	451.72	475.81	8.34
PP/BF/T3	301.32	444.00	353.97	452.11	475.37	9.94
PP/BF/T4	297.51	443.15	353.41	451.52	476.60	8.26

behavior was probably attributed to higher thermal conductivity of TiO_2 nanoparticles resulting in lower thermal decomposition temperature. Furthermore, with the TiO_2 nanoparticles mass ratio increased from 0.1% to 0.8%, the thermal decomposition temperature in both the stages of the samples had no obvious change, which indicated that there was no substantial difference in the interaction between the components of the PP/BFs composites. The residual weight (W_r) at 600 °C increased gradually with the existence of TiO_2 nanoparticles in PP/BFs composites, which indicated that the thermal degradation of BFCs became more difficult due to the interface enhancement between the BFs and matrix, as well as the nondecomposition characteristic of TiO_2 nanoparticles, which is in line with the literature [37–40].

Dynamic mechanical analysis (DMA)

DMA is often used to study relaxations in polymeric composites [41]. We can get a clear result about the matrix/fiber–filler interactions by investigating the dynamic mechanical properties of the PP/BFs composites. Figure 6a–c shows the dynamic mechanical analysis curves of the PP/BFs composites with increase in temperature.

Storage modulus (E′)

The variation of storage modulus (E') as a function of temperature for different samples is presented in Fig. 6a. The E' values of composites exhibited the same tendency as the matrix PP resin. It was evident that the PP/BFs composites presented a higher storage modulus in comparison with pure PP over the entire temperature range of the study (−20 to 120 °C). For the pure PP, the highest E' value was 2751 MPa, whereas for the PP/BF composite the value was increased to 4020 MPa. This behavior was primarily attributed to the addition of high surface rigid BFs into semi-rigid PP matrix effectively enhancing the stiffness of samples. However, in case of the treated PP/BFs composites a slight reduced E' value was observed. In all the systems, we also observed the E′ values of the composites dropped with increasing temperature due to softening of PP matrix and increasing of molecular mobility [42]. Similar trend for polypropylene sisal biocomposites was reported by Bassyouni et al. [43]. For PP/BFs composites, the E' value gradually increased from 3898 to 3998 MPa with increased content of TiO_2 nanoparticles from 0.1% to 0.8%. The highest E' value of PP/BFs composites compared to other samples was primarily attributed to effect caused by the presence of more stiff TiO2 nanoparticles, which was similar to the

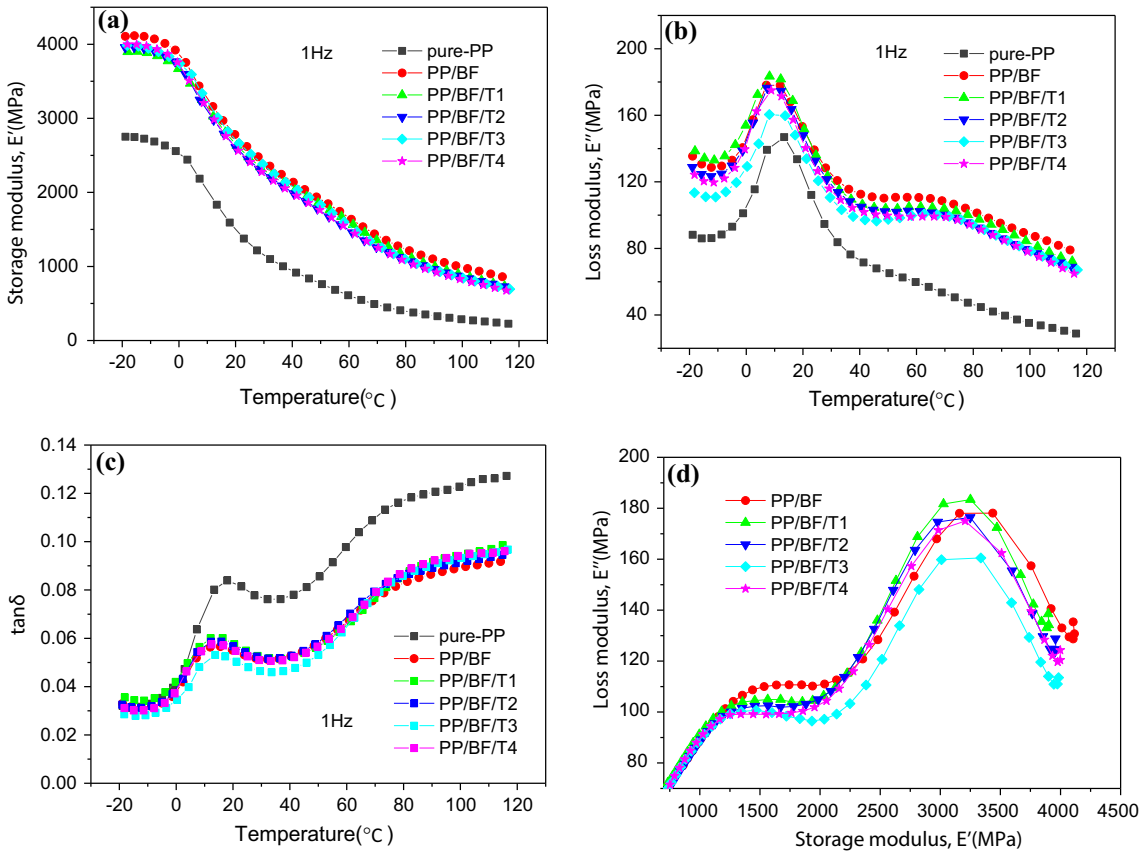

Figure 6 DAM measurement of PP/BFs composites under loading frequency of 1 Hz: **a** storage modulus (E'), **b** loss modulus (E''), **c** damping factor (tan δ) and **d** Cole–Cole plots.

results reported in the use of different matrix and inorganic fillers by Sanjay et al. [44] and Kodgire et al. [45].

Loss modulus (E″)

Figure 6b shows a relationship between temperature and loss modulus (E'') of PP/BFs composites. Similar to E' values, the E'' values of the composites enhanced significantly with the incorporation of BFs compared to neat PP matrix. The E'' curves of all samples exhibited a single prominent peak at approximately 15 °C, which corresponded to the glass-transition temperature (T_g) of samples. The E'' value was 146.9 MPa for pure PP, which significantly increased to 189.3 MPa for PP/BF composite and to 183.4 MPa for PP/BF/T1 composites. This increment in E'' values of the composites with addition of BFs can be attributed to high energy losses as a result of interfacial friction existing between the BFs and matrix [46], as well as maximum viscous dissipation [35].

In case of addition of BFs treated by TiO_2 nanoparticles, it was evident that the treated composites showed a lower E'' values compared to the PP/BF composite throughout the whole temperature range. A decrease in E'' value was attributed to the lower mobility of the matrix molecules caused by the addition of stiff TiO_2 nanoparticles that led to a decreasing in toughness and energy absorption capability of the composites. However, with further increase in temperature (about 70–80 °C), it can be observed from Fig. 6b that the E'' values of the PP/BFs composites were not much difference and slowly decreased, which was mainly attributed to the movement of the matrix molecules in the noncrystalline part of the crystalline region. The PP/BFs composites were in rubber state in this temperature range [47, 48].

Damping factor (tan δ)

Damping factor (tan δ) is the ratio of loss modulus to the storage modulus (E''/E'), and it represents the

Table 5 Parameters of DMA for PP/BFs composites at frequency of 1 Hz

Parameters	Pure-PP	PP/BF	PP/BF/T1	PP/BF/T2	PP/BF/T3	PP/BF/T4
tan δ_{max}	0.08394	0.06025	0.06005	0.05865	0.05247	0.05703
T_g (°C)	13.39	15.12	15.4	15.91	17.26	16.56
C	-	0.488	0.495	0.524	0.530	0.528

Note tan δ_{max} corresponding to grass-transition temperature (T_g) was reported

energy dissipation capability of a viscoelastic material. The variation of tan δ of neat PP and PP/BFs composites as a function of temperature at 1 Hz is shown in Fig. 6c. It was observed that the magnitude of tan δ of neat PP and PP/BFs composites increased with an increase in the temperature, whereas the incorporation of BFs or TiO_2 nanoparticles reduced the tan δ value of pure PP (Table5). This was attributed to the substantial increment in storage modulus in comparison with that of the loss modulus, and this enhancement in stiffness of the composites could be ascribed to high stiffness of the BFs and TiO_2 nanoparticles. Besides, the BFs restricted the mobility of PP molecules in the relaxation process [46]. Similar behavior of tan δ values of PP/jute fiber composites had been reported by Doan et al. [49]. In addition, the phenomenon of T_g shifted slightly to higher temperature with the addition BFs and nanofillers to composites in comparison with pure PP was observed. The PP/BF/T3 composite performed the highest T_g, which was 17.26 °C. This shift to higher temperature was attributed to the restriction in the mobility of the polymer chains in the noncrystalline phase resulting in more energy required to occur the transition [35]. This suggested a good bonding at the filler–matrix interface was obtained. Furthermore, the parameter of reinforcement effectiveness coefficient (C) can be employed for quantitative evaluation of the interface adhesion characteristics of the BFs and PP matrix, and its expression is as follows Eq. (1):

$$C = \frac{E'_g/E'_r(\text{composite})}{E'_g/E'_r(\text{matrix})} \quad (1)$$

where E'_g and E'_r are the storage modulus values in the glassy (0 °C) and rubbery (80 °C) regions for the PP/BFs composites or PP matrix, respectively [46].

The C values of the PP/BFs composites are also summarized in Table 5. We found that the PP/BF/T3 composite led to well BFs-matrix interfacial adhesion which resulted in higher C values, which was in accordance with the above research.

Cole–Cole plot

Cole–Cole plot is drawn according to the relationship between loss modulus and storage modulus to provide information about the degree of homogeneity of a composite material system. Researchers have reported that the perfect semicircular Cole–Cole curves represent a homogeneous polymer system with a good dispersion of filler, indicating well adhesion between the fillers and matrix. In contrast, incomplete or elliptic Cole–Cole curves indicate the heterogeneous polymer system and phase segregation. Moreover, the higher degree of Cole–Cole curves transformation to elliptic shape suggests the better interfacial compatibility among the components of the multiphase composite system. Cole–Cole plots of different samples at frequency of 1 Hz are displayed in Fig. 6d. The results showed that all curves represented incomplete semicircular curves, indicating that these polymer systems were heterogeneous. However, the difference between the curves could further illustrate the influence of the addition of TiO_2 nanoparticles on the microstructure changes of PP matrix in the PP/BFs composites. We found that PP/BF/T3 composite demonstrated a relatively narrow curve, while PP/BF composite appeared a wider peak shape. This was a convincing evidence that TiO_2 nanoparticles had an influence on the shape of the Cole–Cole curves and improved the interfacial adhesion properties between BFs and PP matrix in the PP/BFs composites. This finding was very consistent with the results of E', E'' and tan δ in this study. Similarly, several researchers had reported similar opinions in the literature of polymer-based composites [46].

SEM observation

SEM micrographs of the fractured surfaces of the PP/BFs composites reinforced by TiO_2 nanoparticles are displayed at 100 × and 20,000 × magnification in Fig. 7. It can be obviously seen from Fig. 7a that there

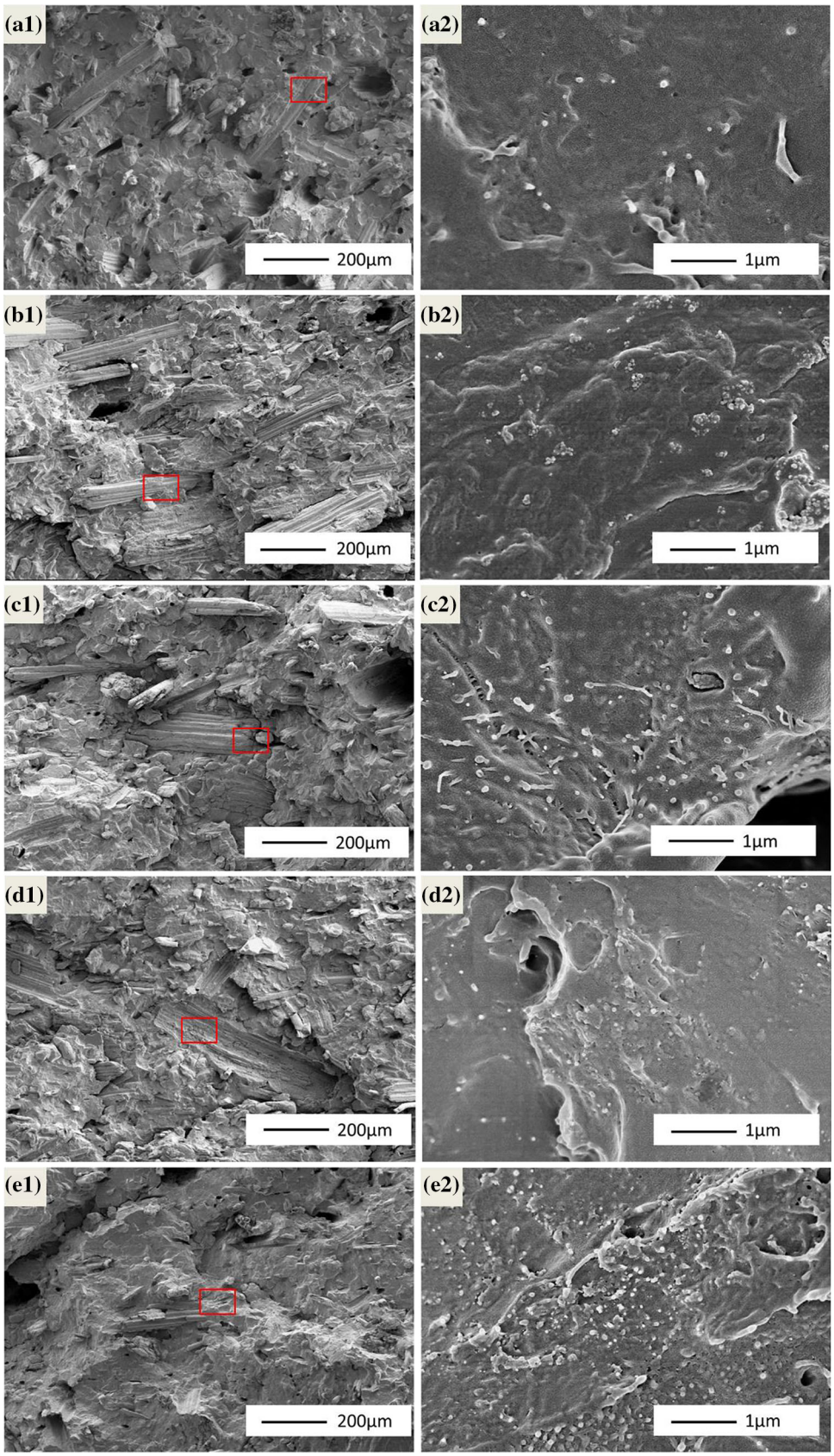

Figure 7 SEM micrographs for the fracture surface of **a** PP/BF composite, **b** PP/BF/T1 composite, **c** PP/BF/T2 composite, **d** PP/BF/T3 composite and **e** PP/BF/T4 composite.

were many cracks and cavities in the interface between the BFs and the PP matrix in the PP/BF composite without any treatment. The BFs agglomerated heavily and were pulled out from the polymer matrix. The fractured surface was smooth and flat, indicating that the interface between the BFs and PP matrix was weak. After adding an appropriate amount of TiO_2 nanoparticles into the PP/BFs composites (Fig. 7b–e), the larger specific surface led to an increase in the interfacial binding between the BFs and matrix with no complete BFs pulled out at the fractured surface. With increased TiO_2 nanoparticles content, the fractured surface became rough and incomplete. In particular, when the TiO_2 nanoparticles loading increased to 0.8 wt%, a number of bigger holes and cracks was found at the interface between the BFs and the PP matrix in the PP/BF/T4 composite (Fig. 7e). Moreover, it was easy to observe from Fig. 7e2 that TiO_2 nanoparticles occurred seriously agglomeration phenomenon in the PP matrix. The phenomenon implied the interface between the BFs and PP matrix might become poor, resulting in the significantly changed morphology of fractured surface. However, Fig. 7d illustrates that there were no cracks and cavities in the fractured surface, indicating stronger interfacial bonding strength between the treated BFs by 0.4wt% TiO_2 nanoparticles and the PP matrix. These results indicated that appropriate TiO_2 nanoparticles enhanced the interfacial adhesion between BFs and PP matrix.

Water absorption test

Water absorption

The water absorption of BPCs plays a crucial role in the mechanical properties and dimensional stability, especially during their use as outdoor construction materials [50]. The influence of TiO_2 nanoparticles on the water absorption values observed in the PP/BFs composites after 24-h and 48-h purified water immersion times is shown in Fig. 8a, b, respectively. As expected, the degree of water absorption in all the samples increased with increasing immersion time. However, with the presence of TiO_2 nanoparticles into the PP/BFs composites the water absorption values exhibited a slight decreasing tendency, which was primarily attributed to the better interface bonding between BFs and matrix through TiO_2 nanoparticles and the reduced hydrophilicity of modified BFs. There are three main pathways about water uptake in BPCs composites, including adsorption and diffusion through the matrix, capillarity through natural fibers and permeation or movement via porosities in the fiber–matrix interface. Therefore, the relative hydrophilicity of the fiber and the matrix, the bonding degree of the fiber and the matrix and the morphology of the composites all affect the water absorption of the BPCs composites. The effect on water absorption of composites made with inorganic fillers had been discussed in many literature [35]. However, in the case of PP/BF/T4 composite, the presence of 0.8wt% TiO_2 nanoparticles slightly increased the water absorption rate of samples. The reason might be that excessive TiO_2 nanoparticles caused agglomeration and changed the distribution of TiO_2 nanoparticles on the surface of

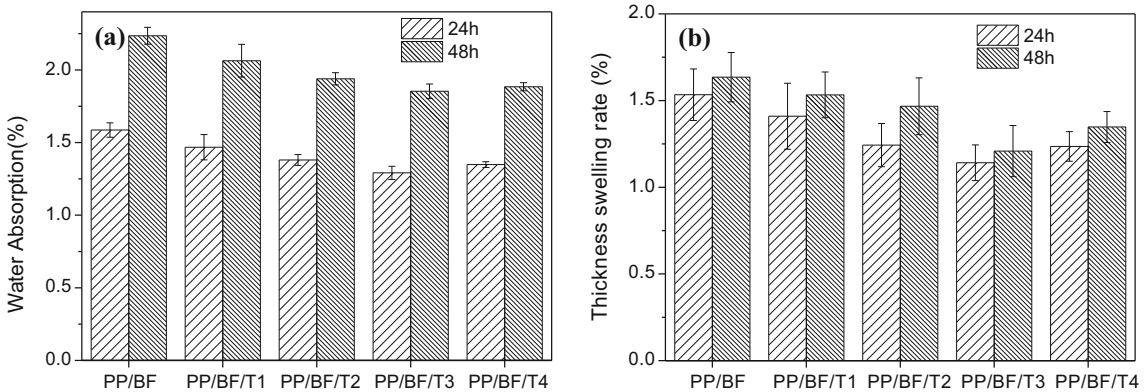

Figure 8 Water absorption tests of the PP/BFs composites after 24 h and 48 h: **a** water absorption, and **b** thickness swelling.

BFs, which made more hydroxyl group exposed on the BFs' surface again and interacted with water molecules. Thus, the water absorption of PP/BF/T4 composite was slightly higher in comparison with PP/BF/T3 composite. Similar result in increased equilibrium water content was also reported in the use of different matrix and nanofillers by Ibrahim [51].

Thickness swelling

Thickness swelling rates of the PP/BFs composites after 24-h and 48-h immersion in purified water are shown in Fig. 8b. The thickness swelling rates of the composites increased with the water absorption and thus had a trend similar to that of the water absorption. Similar results were obtained by other authors [50, 51]. It could be seen that the PP/BF composite had the maximum thickness swelling values (1.53% and 1.63% after 24-h and 48-h water immersion, respectively), while the PP/BF/T3 composite exhibited the smallest thickness swelling rates among other samples (1.14% and 1.21% after 24-h and 48-h water immersion, respectively). This was primarily attributed to the TiO_2 nanoparticles on the surface of BFs acted as barrier and limited the expansion of BFs after absorption of water.

Conclusions

PP/BFs composites were prepared by extrusion and injection molding process, and the effects of TiO_2 nanoparticles on the physical and mechanical properties, dynamic mechanical properties, thermal properties, fracture surface morphology and water absorption of composites were investigated. With the presence of TiO_2 nanoparticles in PP/BFs composites, the mechanical strength of the composites increased slightly. The tensile strength and impact strength of the composite with a 0.4 wt% TiO_2 nanoparticles increased by 5.74% and 4.47% compared with the untreated composite, respectively. The crystallinity and thermal stability of the composites were improved, indicating that the nanoeffect could improve the crystallization behavior of PP matrix. DMA showed that the sample with the combination of 0.4wt% TiO_2 nanoparticles had the higher storage modulus (E') and glassy transition temperature (T_g), and reinforcement effectiveness coefficient (C) was slightly higher than that of other samples. Moreover, with increased TiO_2 nanoparticles content, the fractured surface became rough and caused more microcracks. Besides, compared with the untreated BFs composite, the water absorption and the thickness swelling of the PP/BF/T3 composite were decreased by 17.09% and 26.12% after 48 h of immersion, respectively. These results showed that TiO_2 nanoparticles could enhance the interface bonding strength between BFs and matrix PP.

Acknowledgements

This work has been supported by the financial support from National Natural Science Foundation of China (31770600) and Fujian Natural Science Foundation Key Project (2020J02031).

Supplementary Information: The online version contains supplementary material available at https://doi.org/10.1007/s10853-021-06100-z.

References

[1] Lian C, Liu R, Luo J, Yang F, Zhang S, Fei B (2020) The morphological characteristics and classification of vascular parenchyma cells in bamboo, *Phyllostachys edulis* (Carr.). J Houz Holzforschung 74:1–10. https://doi.org/10.1515/hf-2019-0241

[2] Hsu CY, Yang TC, Wu TL, Hung KC, Wu JH (2018) The influence of bamboo fiber content on the non-isothermal crystallization kinetics of bamboo fiber-reinforced polypropylene composites (BPCs). Holzforschung 72:329–336. https://doi.org/10.1515/hf-2017-0046

[3] Jariwala H, Jain P (2019) A review on mechanical behavior of natural fiber reinforced polymer composites and its applications. J Reinf Plast Comp. https://doi.org/10.1177/0731684419828524

[4] Kumar N, Mireja S, Khandelwal V, Arun B, Manik G (2017) Light-weight high-strength hollow glass microspheres and bamboo fiber based hybrid polypropylene composite: a strength analysis and morphological study. Compos Part B-Eng 109:1–22. https://doi.org/10.1016/j.compositesb.2016.10.052

[5] Liew FK, Hamdan S, Rahman MR, Rusop M, Khan A (2020) Thermo-mechanical properties of jute/bamboo/polyethylene hybrid composites: the combined effects of silane

coupling agent and copolymer. Polym Composite. https://doi.org/10.1002/pc.25755

[6] Xie J, Qi J, Hu T, De Hoop CF, Hse CY, Shupe TF (2016) Effect of fabricated density and bamboo species on physical-mechanical properties of bamboo fiber bundle reinforced composites. J Mater Sci 51:7480–7490. https://doi.org/10.1007/s10853-016-0024-3

[7] Safwan A, Jawaid M, Sultan MTH, Hassan A (2018) Preliminary study on tensile and impact properties of Kenaf/bamboo fiber reinforced epoxy composites. J Renew Mater. https://doi.org/10.7569/JRM.2018.634103

[8] Depuydt DEC, Billington L, Fuentes C, Sweygers N, Dupont C, Appels L, Ivens J, Van VAW (2019) European bamboo fibres for composites applications, study on the seasonal influence. Ind Crops Prod 133:304–316. https://doi.org/10.1016/j.indcrop.2019.03.026

[9] Wang F, Yang M, Zhou S, Ran S, Zhang J (2018) Effect of fiber volume fraction on the thermal and mechanical behavior of polylactide-based composites incorporating bamboo fibers. J Appl Polym Sci 135:46148. https://doi.org/10.1002/app.46148

[10] Zakikhani P, Zahari R, Sultan MTH, Majid DL (2014) Extraction and preparation of bamboo fibre-reinforced composites. Mater Design 63:820–828. https://doi.org/10.1016/j.matdes.2014.06.058

[11] Mahir FI, Keya KN, Sarker B, Nahiun KM, Khan RA (2019) A brief review on natural fiber used as a replacement of synthetic fiber in polymer composites. Mater Eng Res 1:88–99. https://doi.org/10.25082/MER.2019.02.007

[12] Biswas S, Shahinur S, Hasan M, Ahsan Q (2015) Physical, mechanical and thermal properties of jute and bamboo fiber reinforced unidirectional epoxy composites. Proc Eng 105:933–939. https://doi.org/10.1016/j.proeng.2015.05.118

[13] Li Y, Jiang LY, Xiong CD, Peng WJ (2015) Effect of different surface treatment for bamboo fiber on the crystallization behavior and mechanical property of bamboo fiber/nanohydroxyapatite/poly(lactic-co-glycolic) composite. Ind Eng Chem Res 54:12017–12024. https://doi.org/10.1021/acs.iecr.5b02724

[14] Tang S, Jiang L, Ma B, Tang C, Su S (2020) Preparation and characterization of bamboo fiber/chitosan/nano-hydroxyapatite composite membrane by ionic crosslinking. Cellulose 4:1–12. https://doi.org/10.1007/s10570-020-03145-2

[15] Wang CC, Cai L, Shi SQ, Wang G, Cheng HT, Zhang SB (2019) Thermal and flammable properties of bamboo pulp fiber/high-density polyethylene composites: influence of preparation technology, nano calcium carbonate and fiber content. Renewable Energy 134(4):436–445. https://doi.org/10.1016/j.renene.2018.09.051

[16] Fei P, Xiong HG, Cai J, Liu C, Zia-ud-Din YuY (2016) Enhanced the weatherability of bamboo fiber-based outdoor building decoration materials by rutile nano-TiO_2. Constr Build Mater 114:307–316. https://doi.org/10.1016/j.conbuildmat.2016.03.166

[17] Chaudhary V, Ahmad F (2020) A review on plant fiber reinforced thermoset polymers for structural and frictional composites. Polym Testing 91:106792. https://doi.org/10.1016/j.polymertesting.2020.106792

[18] Rahman MR, Hamdan S, Hashim DMA, Islam MS, Takagi H (2015) Bamboo fiber polypropylene composites: effect of fiber treatment and nano clay on mechanical and thermal properties. J Vinyl Addit Techn 21:253–258. https://doi.org/10.1002/vnl.21407

[19] Pradeep KK, Rakesh K (2011) Reinforcing effect of nanoclay in bamboo-reinforced thermosetting resin composites. Polym Plast Technol 50:127–135. https://doi.org/10.1080/03602559.2010.512350

[20] Wang J, Dong J, Zhang J, Zhu B, Cui D (2018) Effects of fiber-surface modification on the properties of bamboo flour/polypropylene composites and their interfacial compatibility. J Polym Eng 38:157–166. https://doi.org/10.1515/polyeng-2016-0432

[21] Zuo Y, Chen K, Li P, He X, Li W, Wu Y (2020) Effect of nano-SiO_2 on the compatibility interface and properties of polylactic acid-grafted-bamboo fiber/polylactic acid composite. Int J Biol Macromol 157:177–186. https://doi.org/10.1016/j.ijbiomac.2020.04.205

[22] Abeer AS, Rozli Z, Che HA (2020) Tensile properties and microstructure of single-cellulosic bamboo fiber strips after alkali treatment. Fibers 8:26. https://doi.org/10.3390/fib8050026

[23] Chen H, Yu Y, Zhong TH, Wu Y, Li YJ, Wu ZH, Fei BH (2017) Effect of alkali treatment on microstructure and mechanical properties of individual bamboo fiber. Cellulose 24:333–347. https://doi.org/10.1007/s10570-016-1116-6

[24] Lee SY, Kang IA, Park BS, Doh GH, Park BD (2008) Effects of filler and coupling agent on the properties of bamboo fiber-reinforced polypropylene composites. J Reinf Plast Compos 9:1–17. https://doi.org/10.1177/0731684408094070

[25] del Pilar L, Cabrera F, de Lima R, Santana MC, Chamorro CD (2020) Influence of coupling agent in mechanical, physical and thermal properties of polypropylene/bamboo fiber composites: under natural outdoor aging. Polymers 12:929. https://doi.org/10.3390/polym12040929

[26] Li YJ, Yin LP, Huang CJ, Meng YJ, Fu F, Wang SQ, Wu Q (2015) Quasi-static and dynamic nanoindentation to determine the influence of thermal treatment on the mechanical properties of bamboo cell walls. Holzforschung 69:909–914. https://doi.org/10.1515/hf-2014-0112

[27] Akinyemi AB, Omoniyi ET, Onuzulike G (2020) Effect of microwave assisted alkali pretreatment and other pretreatment methods on some properties of bamboo fibre reinforced cement composites. Constr Build Mater 245:118405. https://doi.org/10.1016/j.conbuildmat.2020.118405

[28] Cheng HT, Gao J, Wang G, Shi SQ, Zhang SB, Cai LP (2015) Enhancement of mechanical properties of composites made of calcium carbonate modified bamboo fibers and polypropylene. Holzforschung 69:215–221. https://doi.org/10.1515/hf-2014-0020

[29] Ying SJ, Wang CB, Lin Q (2013) Effects of heat treatment on the properties of bamboo fiber/polypropylene composites. Fiber Polym 14:1894–1898. https://doi.org/10.1007/s12221-013-1894-5

[30] Inácio André LN, Nonato Renato C, Bonse Baltus C (2017) Recycled PP/EPDM/talc reinforced with bamboo fiber: Assessment of fiber and compatibilizer content on properties using factorial design. Polym Test 61:214–222. https://doi.org/10.1016/j.polymertesting.2017.05.022

[31] Abdul Khalil HPS, Bhat IUH, Jawaid M, Zaidon A, Hadi YS (2012) Bamboo fibre reinforced biocomposites: a review. Mater Des 42:353–368. https://doi.org/10.1016/j.matdes.2012.06.015

[32] Sun ZY, Wu MM (2019) Effects of sol-gel modification on the interfacial and mechanical properties of sisal fiber reinforced polypropylene composites. Ind crops prod 137:89–97. https://doi.org/10.1016/j.indcrop.2019.05.021

[33] Deng JC, Wei X, Zhou HY, Wang G, Zhang SB (2020) Inspiration from table tennis racket: preparation of rubber-wood-bamboo laminated composite (RWBLC) and its response characteristics to cyclic perpendicular compressive load. Compos Struct 241:112135. https://doi.org/10.1016/j.compstruct.2020.112135

[34] Nigel C, Paula D, Derya K, Jaipal G, Tony M (2018) Isothermal and non-isothermal crystallization kinetics of composites of poly(propylene) and MWCNTs. Adv Ind Eng Polymer Res 1:99–110. https://doi.org/10.1016/j.aiepr.2018.06.001

[35] Sukanya S, Raju VSK (2018) Mechanical, dynamic mechanical and thermal properties of banana fiber/recycled high density polyethylene biocomposites filled with flyash cenospheres. J Polym Environ 1:200. https://doi.org/10.1007/s10924-017-0938-0

[36] Zahedi M, Khanjanzadeh H, Pirayesh H, Saadatnia MA (2015) Utilization of natural montmorillonite modified with dimethyl, dehydrogenated tallow quaternary ammonium salt as reinforcement in almond shell flour–polypropylene bio-nanocomposites. Compos Part B-Eng 71:143–151. https://doi.org/10.1016/j.compositesb.2014.11.009

[37] Wang ZD, Yang MM, Cheng YH, Liu JY, Xiao B, Chen SY, Huang JL, Xie Q, Wu GL, Wu HJ (2019) Dielectric properties and thermal conductivity of epoxy composites using quantum-sized silver decorated core/shell structured alumina/polydopamine. Compos A 118:302–311. https://doi.org/10.1016/j.compositesa.2018.12.022

[38] Pan C, Kou KC, Zhang Y, Li ZY, Wu GL (2018) Enhanced through-plane thermal conductivity of PTFE composites with hybrid fillers of hexagonal boron nitride platelets and aluminum nitride particles. Compos B 153:1–8. https://doi.org/10.1016/j.compositesb.2018.07.019

[39] Pan C, Kou KC, Jia Q, Zhang Y, Wu GL, Ji TZ (2017) Improved thermal conductivity and dielectric properties of hBN/PTFE composites via surface treatment by silane coupling agent. Compos B Eng 111:83–90. https://doi.org/10.1016/j.compositesb.2016.11.050

[40] Pan C, Zhang JQ, Kou KC, Zhang Y, Wu GL (2018) Investigation of the through-plane thermal conductivity of polymer composites with in-plane oriented hexagonal boron nitride. Int J Heat Mass Tran 120:1–8. https://doi.org/10.1016/j.ijheatmasstransfer.2017.12.015

[41] Mishra R, Wiener J, Militky J, Petru M, Tomkova B, Novotna J (2020) Bio-composites reinforced with natural fibers: comparative analysis of thermal, static and dynamic-mechanical properties. Fiber Polym 21:619–627. https://doi.org/10.1007/s12221-020-9804-0

[42] Saba N, Jawaid M, Alothman OY, Paridah MT (2016) A review on dynamic mechanical properties of natural fibre reinforced polymer composites. Constr Build Mater 106:149–159. https://doi.org/10.1016/j.conbuildmat.2015.12.075

[43] Bassyouni M (2018) Dynamic mechanical properties and characterization of chemically treated sisal fiber-reinforced polypropylene biocomposites. J Reinf Plast Compos 37:1402–1417. https://doi.org/10.1177/0731684418798049

[44] Sanjay MR, Jyotishkumar Parameswaranpillai SS, Jawaid M, Pruncu CI, Khan A (2019) A comprehensive review of techniques for natural fibers as reinforcement in composites: preparation. Process Charact Carbohydr Polym 11:108. https://doi.org/10.1016/j.carbpol.2018.11.083

[45] Kodgire P, Kalgaonkar R, Hambir S, Bulakh N (2010) PP/Clay nanocomposites: effect of clay treatment on morphology and dynamic mechanical properties. J Appl Polym Sci 81:1786–1792. https://doi.org/10.1002/app.1611

[46] Karaduman Y, Sayeed MMA, Onal L, Rawal A (2014) Viscoelastic properties of surface modified jute fiber/polypropylene nonwoven composite. Compos Part B-Eng 67:111–118. https://doi.org/10.1016/j.compositesb.2014.06.019

[47] Etaati A, Pather S, Fang Z, Wang H (2014) The study of fibre/matrix bond strength in short hemp polypropylene composites from dynamic mechanical analysis. Compos Part B-Eng 62:19–28. https://doi.org/10.1016/j.compositesb.2014.02.011

[48] Nayak SK, Mohanty S, Samal SK (2009) Influence of short bamboo/glass fiber on the thermal, dynamic mechanical and rheological properties of polypropylene hybrid composites. Mat Sci Eng A-Struct 523:32–38. https://doi.org/10.1016/j.msea.2009.06.020

[49] Doan T-T-L, Brodowsky H, Mäder E (2007) Jute fibre/polypropylene composites II. Thermal, hydrothermal and dynamic mechanical behaviour. Compos Sci Technol 67:2707–2714. https://doi.org/10.1016/j.compscitech.2007.02.011

[50] Zahedi M, Pirayesh H, Khanjanzadeh H, Tabar MM (2013) Organo-modified montmorillonite reinforced walnut shell/polypropylene composites. Mater Design 51:803–809. https://doi.org/10.1016/j.matdes.2013.05.007

[51] Ibrahim ID, Jamiru T, Sadiku RE, Kupolati WK, Agwuncha SC (2016) Dependency of the mechanical properties of sisal fiber reinforced recycled polypropylene composites on fiber surface treatment. Fiber Content Nanoclay J Polym Environ 25:427–434. https://doi.org/10.1007/s10924-016-0823-2